Numerical Stabilities and Post-Buckling Responses in Large Steps of Baraff-Witkin Cloth Simulation

YIBO JIAO, University of British Columbia, Canada

ACM Reference Format:
Yibo Jiao. 2020. Numerical Stabilities and Post-Buckling Responses in Large Steps of Baraff-Witkin Cloth Simulation. 1, 1 (December 2020), 8 pages. https://doi.org/10.1145/nnnnnnn.nnnnnnn

1 ABSTRACT

Particle-based physical model of fabrics simulations with fixed large time step use implicit integration methods or backward Euler to solve the linear system. Implicit cloth simulation techniques overcome the numerical instability caused by explicit methods which requires small time step. Baraff and Witkin initially introduced the simulation system which models shear and stretch force with techniques of adding damping forces and enforcing constraints on individual cloth particles in their paper *Large Steps in Cloth Simulation* published in 1998. In Choi and Ko's 2002 paper *Stable but responsive cloth*, they present new techniques for modelling compressive forces which are responsible for post-buckling responses of the fabric. In this implementation, I will present a particle-based mass-spring cloth simulation that takes Baraff-Witkin as inspiration and basic framework, and model Choi and Ko's solution for post-buckling response of the cloth. In this report, I will introduce the progress I made to simulate Choi-Ko cloth with implementation and numerical analysis as a course project of CPSC535P offered in 2020 winter term1 in University of British Columbia.

2 INTRODUCTION

In both Baraff and Witkin and Choi and Ko's paper, the simulations are both formulated as time-varying particle differential equation. For a Baraf-Witkin cloth, forces on each particle is modeled in 5 different types: stretch, shear, bending, artificial force and additional damping force. Baraff and Witkin used this additional damping force to overcome the possible numerical instability of their computed linear system. So far, Baraff-Witkin cloth had characterized properties of fabrics by solving this ordinary differential equation. However, another property of animating the fabrics is the cloth's buckling behavior, which is not well characterized by Baraff-Witkin cloth. Since an animation without having such a property will look unnatural, Choi and Ko introduced solutions for predicting post-buckling deformation energy with reasonable assumption to model the out-of-plane wrinkle formulation and solve post-buckling response. With modified Baraf-Witkin cloth's implicit integration method and solutions of post-buckling response, such simulation of cloth is very stable yet also responsive.

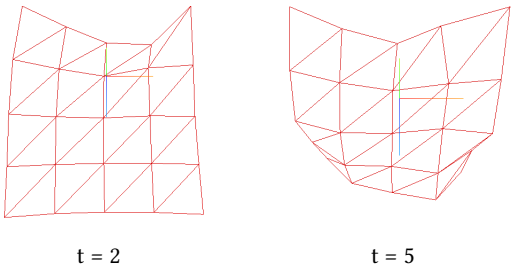

Fig. 1. Sample Result of Grid 4×4 Baraff-Witkin Cloth

In the previous assignment of CPSC535P coursework, a highly simplified version of Baraff-Witkin cloth is implemented, although with low resolution, the simulation of the Baraff-Witkin cloth is only in grid of 4×4, the concept of the particle based model is clear: particle-based simulation of Baraff-Witkin cloth takes each triangular mesh of the cloth and update calculated force by deformation gradient $F = \frac{dX}{dx}$, where X is particle positions in material spaces, and x is particle positions in physical spaces.

3 RELATED WORK

In Baraff and Witkin's paper *Large Steps in Cloth Simulation*, instead of postulating a force acting on each particle, they introduced a constrained condition on each particle. However, the most popular way to implement the Baraff-Witkin cloth is face-based. Baraff and Witkin implemented the simulator which models the triangular mesh. The condition vector is calculated with the deformation gradient and is applied on each face of the triangle.

Baraff and Witkin introduced stretch, shear, bending and damping forces. With bending forces modeled by Baraff and Witkin, bending forces are applied on the two interlaced particles, which properties are similar as buckling. However, there is a conceptual difference between bending and buckling: bending is a state of stress while buckling is the state of instability. Bending always occurs in flexural members like beam and slabs, while column mostly faces buckling behaviour because, upon axial loads on the column, the column becomes unstable due to greater load.

Thus, the bending force cannot model the post-buckling behavior of the cloth, also the stretch and shear forces. For Baraff-Witkin cloth, the purpose of adding damping force is to model in-plane damping to avoid numerical instability of the ordinary differential equation. However, such approach did not focus on buckling behavior of the cloth, which can be observed on their results in which the wrinkles

Author's address: Yibo Jiao, University of British Columbia, Vancouver, BC, Canada.

XXXX-XXXX/2020/12-ART $15.00
https://doi.org/10.1145/nnnnnnn.nnnnnnn

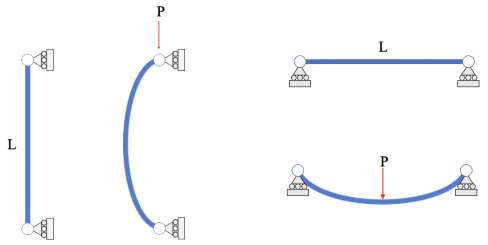

Buckling Bending

Fig. 2. Buckling and Bending of the Column

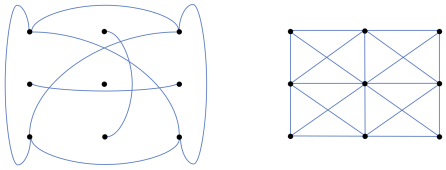

Interlaced Connections Sequential Connections

Fig. 3. All Connections of a 3 Cloth

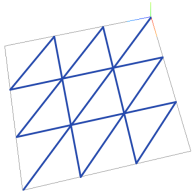

(a) Inner Connections of 3 × 3 Baraff-Witkin Cloth Mesh

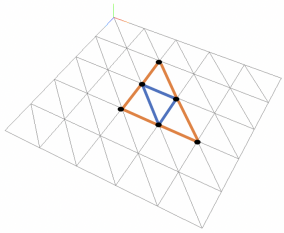

(b) Adjacent Faces For Updating Bending Forces

Fig. 4. Baraff-Witkin Cloth Connections

on the fabric were not well simulated. To implement Choi and Ko's *Stable but Responsive Cloth*, it is crucial to experiment and analysis the buckling property of the particles. For the implementation of the Choi-Ko cloth, different from Baraff-Witkin Cloth, Choi-Ko Cloth updates forces in particle-based approach.

4 METHODS AND ANALYSIS

Choi and Ko introduced interacting particle systems to model particles of the mesh and handling buckling problem. There are two types of interactions which correspond two types of connections in the interacting particle system. Type1 interactions are responsible for stretch and shear resistance and Type2 interactions are responsible for compression resistance.

4.1 Interactive Particles

Type1 interactions connect $P(i, j)$ with $P(i \pm 1, j), P(i, j \pm 1), P(i \pm 1, j \pm 1)$, called sequential connections.
Type2 interactions connect$P(i, j)$ with $P(i \pm 2, j), P(i, j \pm 2), P(i \pm 2, j \pm 2)$, called interlaced connections.
For a 3×3 cloth, all connections are shown in figure 3 above, to avoid complexity of large mesh, I only present this smallest size. In addition, it is valuable to calculated the number of connections with the size of the cloth, assume that we only have square clothes, the size of the cloth is $N \times N$. Let C be the number of the connections of one single type:

$$C = \begin{cases} 2(N-1)(2N-1) & type = sequential \\ 4(N-1)(N-2) & type = interlaced \end{cases}$$

We can conclude that both of the number of the connections of each type is in $O(N^2)$, therefore, the simulator will have a render loop of updating $O(N^2)$ forces as well as $O(N^2)$ iterations for each time step. Compared to the naive implementation (triangular-faces based) of the Baraff-Witkin cloth, each render loop of their simulator will have an iteration number dependent on the number of the mesh's total number of triangular faces. For stretch and shear forces, we only need to update forces for each vertices of each triangular face, but for bending forces, the acting forces are applied on adjacent triangular faces. To calculate the number of bending forces updating, the number of distinct pair of adjacent triangular faces is equal to the number of connections of the wire frame of the Baraff-Witkin cloth subtract the number of connections on the boundary. The inner connection is the blue connections in Fig4(a).
Thus, we calculated the number of triangular faces given the same assumption as Choi-Ko cloth, denote the total number of updating forces as T:

$$T = \begin{cases} 2(N-1)^2 & type = stretch/shear \\ 2N(N-1) + (N-1)^2 & type = bending \end{cases}$$

We can now calculate the total number of iterations for each rendering loop of Choi-Ko cloth and Baraff-Witkin cloth, denote the number of total iterations of Choi-Ko cloth as CK, and Baraff-Witkin cloth as BW:

$$\begin{cases} CK = 8N^2 - 18N + 10 \\ BW = 5N^2 - 8N + 3 \end{cases}$$

As the plot of two functions of the number of iterations varying with increasing size of the cloth shows, the Choi-Ko cloth always runs slower than the Baraff-Witkin cloth, which explain the phenomenon that naive implementation of Baraff-Witkin simulator runs faster with same particle systems compared to Choi-Ko's implementation.

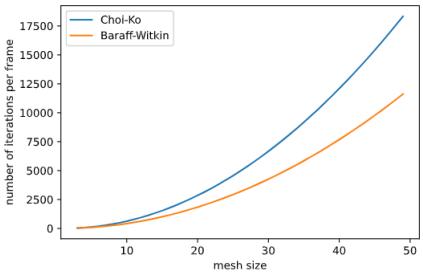

Fig. 5. Running Cost of Two Clothes

4.2 Forces and Energy Function Derivatives

Choi-Ko cloth introduces 3 types of forces, the first two types of forces correspond to the two types of connections in section 4.1. The sequential connections of adjacent particles are responsible for stretch and shear forces, and the interlaced connections of every other particles are responsible for post-buckling behavior and flexural and compressive resistance. In the following sections, the derivation of derivatives of energy function and forces along with analysis of column buckling are provided.

4.3 Type1 Interaction

Type1 interactions act like standard simple linear spring model:

$$f_i = \begin{cases} k_s(|x_{ij}| - L)\frac{x_{ij}}{|x_{ij}|} & : |x_{ij}| \geq L \\ 0 & : |x_{ij}| \geq L \end{cases} \tag{1}$$

$$\frac{\partial f_i}{\partial x_j} = \begin{cases} k_s\left(\frac{x_{ij}x_{ij}^T}{|x_{ij}|^2} + (1 - \frac{L}{|x_{ij}|})(I - \frac{x_{ij}x_{ij}^T}{|x_{ij}|^2})\right) & : |x_{ij}| \geq L \\ 0 & : |x_{ij}| \geq L \end{cases} \tag{2}$$

where k_s is stiff constant, L is rest length of each connection and $x_{ij} = x_j - x_i$.

For equation (1), the stretching force is the derivative of the energy function:

$$E = \frac{1}{2}k_s(|x_{ij}| - L)^2 \tag{3}$$

The stretch/shear energy is the same as applying Hooke's Law on the sequential connections, $|x_{ij} - L|$ models the amount of the free end of the spring was displaced from its relaxed position with length L. Then derivative of energy at particle i is:

$$\frac{\partial E}{\partial x_i} = \frac{\partial E}{\partial |x_{ij}|}\frac{\partial |x_{ij}|}{\partial x_i} = k_s(|x_{ij}| - L)\frac{\partial |x_{ij}|}{\partial x_i}$$

Now calculate the derivative of $\frac{\partial |x_{ij}|}{\partial x_i}$:

$$\begin{aligned} \frac{\partial |x_{ij}|}{\partial x_i} &= \frac{\partial}{\partial x_i}\sqrt{(x_{j1} - xi1)^2 + (x_{j2} - xi2)^2 + (x_{j3} - xi3)^2} \\ &= \frac{1}{2|x_{ij}|}\begin{bmatrix} -2(x_{j1} - x_{i1}) \\ -2(x_{j2} - x_{i2}) \\ -2(x_{j3} - x_{i3}) \end{bmatrix} \\ &= -\frac{x_j - x_i}{|x_{ij}|} \\ &= -\frac{x_{ij}}{|x_{ij}|} \end{aligned} \tag{4}$$

With $\frac{\partial |x_{ij}|}{\partial x_i} = -\frac{x_{ij}}{|x_{ij}|}$ and $f_i = -\frac{\partial E}{\partial x_i}$, we will have the equation same as equation (1) when $|x_{ij}| > L$,

$$f_i = k_s(|x_{ij}| - L)\frac{x_{ij}}{|x_{ij}|}$$

Now, to compute Jacobian matrix for stretch and shear force:

$$\begin{aligned} \frac{\partial f_i}{\partial x_j} &= \frac{\partial}{\partial x_j}k_s(|x_{ij}| - L)\frac{x_{ij}}{|x_{ij}|} \\ &= k_s\left(\frac{\partial}{\partial x_j}(|x_{ij}| - L)\frac{x_{ij}}{|x_{ij}|} + (|x_{ij}| - L)\frac{\partial}{\partial x_j}\frac{x_{ij}}{|x_{ij}|}\right) \end{aligned} \tag{5}$$

We first compute $\frac{\partial}{\partial x_j}(|x_{ij}| - L)$:

$$\frac{\partial}{\partial x_j}(|x_{ij}| - L) = \frac{\partial}{\partial x_j}|x_{ij}| = -\frac{x_{ji}}{|x_{ij}|} = \frac{x_{ij}}{|x_{ij}|} \tag{6}$$

Now compute $\frac{\partial}{\partial x_j}\frac{x_{ij}}{|x_{ij}|}$:

$$\begin{aligned} \frac{\partial}{\partial x_j}\frac{x_{ij}}{|x_{ij}|} &= \frac{\frac{\partial}{\partial x_j}x_{ij}|x_{ij}| - x_{ij}\frac{\partial}{\partial x_j}|x_{ij}|}{|x_{ij}|^2} \\ &= \frac{|x_{ij}| - \frac{x_{ij}x_{ij}^T}{|x_{ij}|}}{|x_{ij}|^2} = \frac{\mathrm{I}}{|x_{ij}|} - \frac{x_{ij}x_{ij}^T}{|x_{ij}|^3} \end{aligned} \tag{7}$$

With combination of equation (5),(6),(7), we will have the equation same as equation (2) when $|x_{ij}| > L$,

$$\frac{\partial f_i}{\partial x_j} = k_s\frac{x_{ij}x_{ij}^T}{x_{ij}^T x_{ij}} + k_s\left(1 - \frac{L}{|x_{ij}|}\right)\left(\mathrm{I} - \frac{x_{ij}x_{ij}^T}{x_{ij}^T x_{ij}}\right)$$

Thus, the derivative of the type1 force gives both along the direction of the connection and the orthogonal direction of the connection. For illustration, the first term of the derivative shows the stiffness along the spring direction. The second term of the derivative tells the stiffness orthogonal to the spring direction. To prove the direction of the stiffness of the derivatives, we multiply x_{ij} on the two terms

$$\frac{x_{ij}x_{ij}^T}{x_{ij}^T x_{ij}}x_{ij} = \frac{x_{ij}x_{ij}^T x_{ij}}{x_{ij}^T x_{ij}} = x_{ij}$$

$$\left(\mathrm{I} - \frac{x_{ij}x_{ij}^T}{x_{ij}^T x_{ij}}\right)x_{ij} = \left(x_{ij} - \frac{x_{ij}x_{ij}^T x_{ij}}{x_{ij}^T x_{ij}}\right) = 0$$

Hence, the inner product of the first term of $\frac{\partial f_i}{\partial x_j}$ and x_{ij} is the same as x_{ij}, and the inner product of the second term of $\frac{\partial f_i}{\partial x_j}$ and x_{ij} is 0. Thus we can conclude that the first term is along the direction of the interaction, the second term is orthogonal to the direction of the interaction. In addition, the second term is vital to the out-of-plane formation, which also contribute to the wrinkle formation of the cloth. From here, we can deduce that using implicit methods for the simulator is necessary for wrinkle formation, since forward Euler method does not need calculations of derivatives of forces and particles $\frac{\partial f_i}{\partial x_j}$, thus explicit methods cannot model out-of-plane wrinkle formations. The same reasoning can also be applied on type2 interactions since type2 derivatives also introduces a term which models the stiffness orthogonal to the connections.

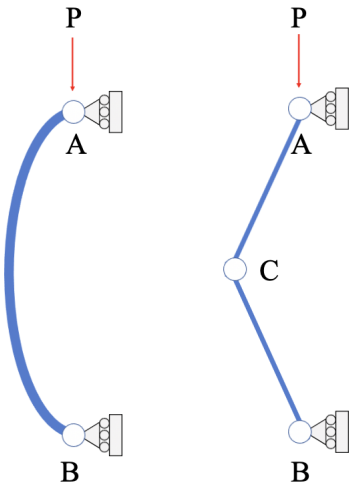

Fig. 6. Model Arches Buckling with Rigid Columns

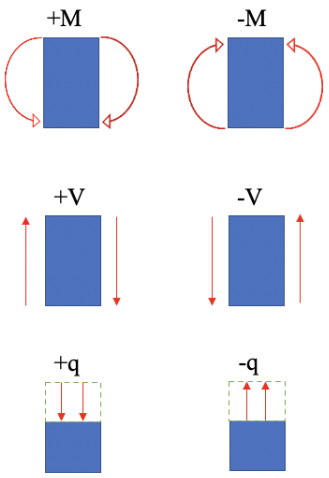

Fig. 7. Moment, Shear Force, Distributed Load of Prismatic Beams

4.4 Buckling Behavior of a Rigid Column

The buckling behavior of the arches shaped beam can be firstly modeled as two rigid column bars with a rotational spring in the middle. As illustrated in Fig 6, consider two rigid columns connected by rotational spring at point C with two ends A, B, and B fixed on the ground. In this configuration, the bending resistance is condensed at point C.

If we add an axially compressive load P along the vertical direction of the column, assume a non-buckling column AB, the compressive resistance will always be along the direction of the connection AB, and the rigid column will be very stable, that explains why the buckling is a state of instability, and the column ABC will be unstable due to the axial loads on the column given that the compressive load is continuously increasing.

To simulate this post-buckling behavior, we should ignore the stable state when the compressive load is small, denote a critical value of the compressive load P_{cr}. At this critical value, the structure is in between the stable state and unstable state, the structure can be either return to the straight position or have lateral displacement, and when P is getting larger, the structure will eventually collapse. Moreover, there is a necessary assumption introduced by Choi and Ko, which is that the fabric is not in the unstable post-buckling state at any time step. This an essential assumption because the unstable buckling state will be corresponding to the returning-back state of the rigid columns. Thus with this assumption, we can evaluate the deformation energy with locally estimated deformed shape, which is explained in the following paragraph. The estimated deformed shape is eventually modeled as circular arcs.

The equation Choi and Ko used to analyze the buckling behavior is the moment equilibrium equation under pinned ends condition, which is evaluated in Gere's 2001 book *Mechanics of Materials*.

In Gere's book, Gere introduced two types of beams, non-prismatic and prismatic beams, the flexural rigidity is denoted as EI. In the case of a non-prismatic beam, the flexural rigidity EI is a variable, and

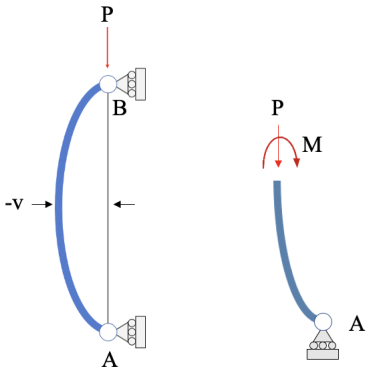

Fig. 8. Column with Pinned Ends

the prismatic beams have constant EI, in our simulation, we model the type2 interaction by prismatic beams to simplify calculations. The differential equations of the prismatic beams are:

$$EI\frac{d^2v}{dx^2} = M$$

$$EI\frac{d^3v}{dx^3} = V$$

$$EI\frac{d^4v}{dx^4} = -q$$

where M is the bending moment, V is the shear force, and q is the distributed load on the prismatic beams, and v is the deflection of the structure. Using primes notation, the equation of the equilibrium we use is $EIv'' = M$.

In order to simplify calculations, by Newton's second law, the two

forces on the same connection will have the same magnitude and opposite directions, hence we only analyze the forces on the pinned end A. The axial force P acting at the cross section is shown in Fig. 8. Since there are no horizontal forces acting at the supports, there are no shear forces in the column. Therefore, from equilibrium of moments about point A, we obtain

$$M + Pv = 0 \quad \text{or} \quad M = -Pv$$

$$EIv'' = -Pv$$

Moreover, since we assume the beam as a prismatic beam, we treat EI as a constant, denoted as k_b, the buckling stiffness.

4.5 Type2 Interaction

Type2 interaction models the solution of post-buckling response by predicting deformation energy from the deformed shape. After experiments, different factors of numerical solutions of the moment equilibrium equation can all be simulated perfectly by circular arcs. Thus Choi and Ko approximated the shape as a circular arc after bending and calculate the curvature to model deformation energy, since the curvature of a circle is easy to compute.
If we treat the deflection as a function, the curvature is the change of tangent vector with respect to the arc-length of the function, hence the curvature will be the second derivative of the deflection v'', thus we obtain

$$k_b\kappa + Pv = 0 \quad \text{or} \quad k_b\kappa = M$$

To formulate the estimated deformation energy, we integrate along the connection spring by the moment:

$$E = \frac{1}{2}\int_0^L M\kappa dx$$

Taking the linear relationship of curvature and bending moment, we obtain:

$$E = \frac{1}{2}\int_0^L M\kappa dx = \frac{1}{2}k_b L\kappa^2$$

Choi and Ko gave the result of the curvature:

$$\kappa = \frac{2}{L}\text{sinc}^{-1}\left(\frac{|x_{ij}|}{L}\right) \tag{8}$$

To prove the formula, we analyze the sector in Fig. 9.: For a circular arc, the curvature of the are is $\frac{1}{R}$, where R is the radius of the sector. Denote the angle between two edges as θ, then we obtain:

$$\begin{aligned}
\frac{L}{R} &= \theta \\
\sin\left(\frac{\theta}{2}\right) &= \frac{\frac{1}{2}|x_{ij}|}{R} \\
\text{sinc}\left(\frac{\theta}{2}\right) &= \sin\left(\frac{\theta}{2}\right)\frac{2}{\theta} \\
&= \frac{|x_{ij}|}{R\theta} = \frac{|x_{ij}|}{L} \\
\text{sinc}^{-1}\left(\frac{|x_{ij}|}{L}\right) &= \frac{\theta}{2} = \frac{L}{2R} \\
\frac{1}{R} &= \frac{2}{L}\text{sinc}^{-1}\left(\frac{|x_{ij}|}{L}\right) = \kappa
\end{aligned}$$

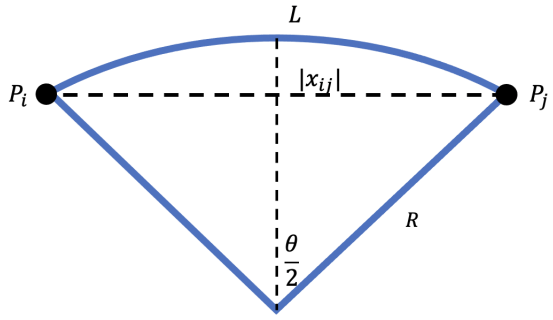

Fig. 9. Sector After Buckling

The buckling force can be formulated by the calculated curvature:

$$f_i = k_b\kappa^2\left(\cos\frac{\kappa L}{2} - \text{sinc}\left(\frac{\kappa L}{2}\right)\right)^{-1}\frac{x_{ij}}{|x_{ij}|} = f_b(|x_{ij}|)\frac{x_{ij}}{|x_{ij}|} \tag{9}$$

To model a realistic phenomenon that buckling happen even if the compressive force is small, we introduced a customized function to simulate the imperfection effect:

$$f_b^* = \max\{f_b, c_b(|x_{ij}| - L)\} \tag{10}$$

where k_b is flexural rigidity, c_b is a constant similar to stiff constant. To derive equation (8), we initially have energy of type2 interaction as:

$$E = \frac{1}{2}k_b L\kappa^2$$

$$f_i = k_b\kappa L\left(\frac{d|x_{ij}|}{d\kappa}\right)^{-1}\frac{x_{ij}}{|x_{ij}|} \tag{11}$$

To compute $\frac{d|x_{ij}|}{d\kappa}$, the trick is to firstly compute the inverse function of equation (8):

$$\begin{aligned}
\frac{\kappa L}{2} &= \text{sinc}^{-1}\left(\frac{|x_{ij}|}{L}\right) \\
\text{sinc}\left(\frac{\kappa L}{2}\right) &= \frac{|x_{ij}|}{L} \\
|x_{ij}| &= L\text{sinc}\left(\frac{\kappa L}{2}\right)
\end{aligned}$$

Now to compute the derivative:

$$\begin{aligned}
\frac{d|x_{ij}|}{d\kappa} &= \frac{L^2}{2}\left(\frac{\frac{\kappa L}{2}\cos\left(\frac{\kappa L}{2}\right) - \sin\left(\frac{\kappa L}{2}\right)}{\left(\frac{\kappa L}{2}\right)^2}\right) \\
&= \frac{L}{\kappa}\left(\cos\left(\frac{\kappa L}{2}\right) - \text{sinc}\left(\frac{\kappa L}{2}\right)\right)
\end{aligned} \tag{12}$$

Combine equation (11) and (12), we will have the equation same as equation (9).

4.6 Polynomial Fit of Sinc

In equation(4), type2 interaction force is modeled by:

$$f_i = k_b \kappa^2 \left(\cos\frac{\kappa L}{2} - \mathrm{sinc}\left(\frac{\kappa L}{2}\right)\right)^{-1} \frac{x_{ij}|}{|x_{ij}|} = f_b(|x_{ij}|)\frac{x_{ij}}{|x_{ij}|}$$

Then function f_b will be parameterized as:

$$f_b(|x_{ij}|) = k_b \kappa^2 \left(\cos\frac{\kappa L}{2} - \mathrm{sinc}\left(\frac{\kappa L}{2}\right)\right)^{-1} \tag{13}$$

If we combine equation (13) with equation (9), i.e. express κ with $|x_{ij}|$, the function f_b is relatively hard to compute its derivative, since Jacobian matrix for Type2 interaction is:

$$\frac{\partial f_i}{\partial x_j} = \frac{df_b^*}{d|x_{ij}|}\frac{x_{ij}x_{ij}^T}{x_{ij}^T x_{ij}}$$

The derivative of $\frac{df_b^*}{d|x_{ij}|}$ must be computed. My implementation solved for this derivative by firstly approximating equation (8), since $|x_{ij}| \le L$ in Type2 interaction, $0 < \frac{|x_{ij}|}{L} \le 1$, then $\mathrm{sinc}^{-1}\left(\frac{|x_{ij}|}{L}\right)$ can be approximate and so as κ, then function f_b can also be approximate by a high degree polynomial function of $|x_{ij}|$.
Similar as Choi and Ko's approach of approximating dependence of f_b on distance between particles, I choose to approximate sinc^{-1} function by a fifth order polynomial.

```
class polysinc:
    # polynomial parameters
    p = None
    # degree
    d = 5

    def __init__(self):
        # linspace of sinc function
        x = np.linspace(0, 1, 1000)
        y = np.sinc(x)
        # get polynomial fit sinc-1
        p = np.polyfit(y, x, self.d)
        f = np.polyval(p, x)
        # scale to normalize the function
        f = self.scale_range(f, 0, 1)
        # re-fit the function values
        p = np.polyfit(x, f, 5)
        self.p = p

    def scale_range (self, f, fmin, fmax):
        f += -(np.min(f))
        f /= np.max(f) / (fmax - fmin)
        f += fmin
        return f
```

From Fig. 11., we have reasonable precise approximation of inverse of sinc function.

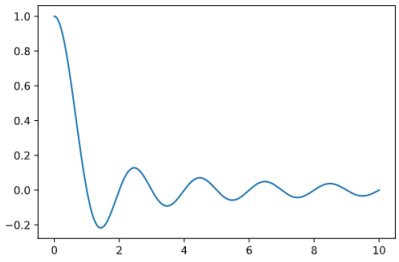

Fig. 10. Sinc Function

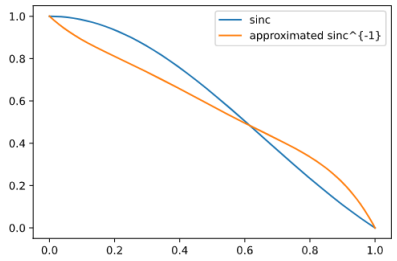

Fig. 11. Approximated Inverse Sinc in Range [0,1]

4.7 Damping

Damping in Choi and Ko paper is easier to implement, since the two types of interactions produces well-conditioned positive definite matrices. To avoid in-plane oscillations, we simply add damping forces as simple linar dampers:

$$f_i = -k_d(v_i - v_j) \tag{14}$$

where k_d is the damping constant.

4.8 Collision Handling

My implementation detects collisions between cloth particles and solid objects with the same approach as Baraff-Witkin cloth, by testing each individual cloth particle against the faces of each solid object, we detect solid-cloth collisions. When a collision is detected, we resist the next time step's displacement along the normal direction of the solid surface and we need to add a frictional force along the tangent direction of the surface.
Moreover, detecting collisions between the cloth and a sphere can have a much easier solution: given a sphere with known radius and center, simply we can iterate all particles and check if the distances between current positions of particles and center of sphere is smaller than the radius. We apply displacement on collided particles along the normal of the sphere. The sample output with a collision handling is in Fig. 12.

4.9 Numerical Methods

For this paper's numerical integration method, Choi and Ko used semi-implicit integration with second-order BDF, the linear system

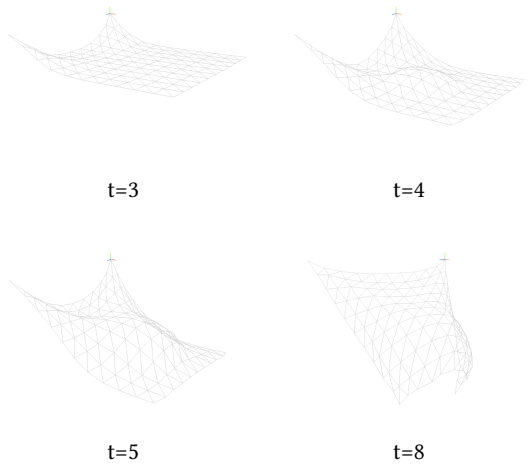

Fig. 12. Solid-Cloth Collision with a Sphere Solid

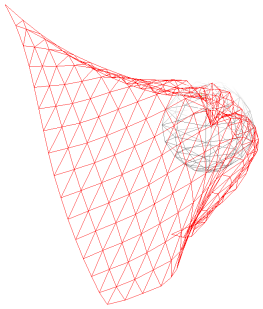

Fig. 13. Instability of Large Time Step Collision Handling

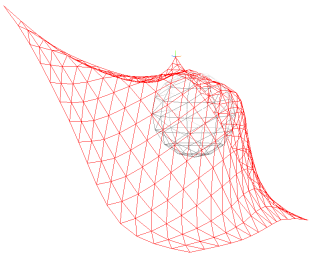

Fig. 14. Collision Handling with Small Time Steps

to solve is:

$$\begin{aligned}
&\left(I - \Delta t \frac{2}{3} M^{-1} \frac{\partial f}{\partial v} - \Delta t^2 \frac{4}{9} M^{-1} \frac{\partial f}{\partial x}\right)(x^{n+1} - x^n) \\
&= \frac{1}{3}(x^n - x^{n-1}) \\
&+ \frac{\Delta t}{9}(8v^n - 2v^{n-1}) \\
&+ \frac{4\Delta t^2}{9} M^{-1}\left(f^n - \frac{\partial f}{\partial v} v^n\right) \\
&- \frac{2\Delta t}{9} M^{-1} \frac{\partial f}{\partial v}(x^n - x^{n-1})
\end{aligned} \tag{15}$$

We solve for x^{n+1}, and f will be the sum of computed Type1, Type2 and damping force at time step n, and Jacobian of $\frac{\partial f}{\partial x}$ and $\frac{\partial f}{\partial v}$ are the sum of Jacobian matrices of Type1 and Type2 and damping respectively also at time step n, and we need two previous state vector to solve for the current time step, i.e. to compute x^{n+1}, we need $x^n, x^{n-1}, v^n, v^{n-1}$. After computing x^{n+1}, we can update v^{n+1} for next iteration.

5 RESULTS

5.1 Code

The coding part of this work is uploaded on github, the link of the repository is: https://github.com/yibojiao/Stable_But_Responsive_Cloth.git

5.2 Parameter Tuning

The magnitude of time step h is highly dependent on the usage of implicit or explicit method. I provide some results with experiments using 10×10 grid cloth with my implementation.

The maximum of time-step using forward Euler, i.e. explicit method is 0.001s, and using implicit method equation given by Choi and Ko can tolerate up to 0.02s time-step. Moreover, it is worth noting that type1, type2 and even damping stiffness constants are also dependent on the numerical methods we use. Usually using backward Euler methods can have much higher stiffness of compressive and stretch resistance, which can produce more wrinkle formations on the cloth, recall that in section 4.3, we conclude that it is hard to model wrinkles with explicit methods since it will require calculations of out-of-plane derivatives, which are generated by the second term of the Jacobian matrix of forces acting on all particles.

However, on the other hand, using large steps can also have some negative effects on solid-cloth collision detecting. For illustration, consider a cloth in section 4.8 which will be colliding with a solid sphere, when a collision is detected, we apply a compensate displacement along the direction of the solid surface normal, if we used a relatively large time step value, it is possible that the current position of the particle is already inside the surface, and the compensation of displacement cannot resist this strict intersection inside the solid, as the rendering loop iterating, the displacement is becoming more and more unstable, as the Fig. 13. shows, some particles near the center of the sphere intersect with the sphere and causes instabilities of the entire structure of the cloth. The Baraff-Witkin solution for solid-cloth collection will be required to compute all nearby particles along with consideration of velocities, which is indeed a perfect solution but at the same time it also brings computational cost. My two solutions for this is: firstly, using very small time-step, in this way, we can even use explicit method to model collision if we do not take buckling behavior as an important contribution to the results; secondly, we can also use a SDF(short for signed distance function), the advantage of using SDF is reducing computational cost, but it will be necessary if we can parameterize the solid surface. For example, for a sphere centered at the origin with radius 1, the function we obtain is:

$$f(x, y, z) = \sqrt{x^2 + y^2 + z^2} - 1$$

Using SDF will only need to check the sign of the current position of particles with the function, for example, we can check some points:

$$f(1,0,0) = 0$$
$$f(0,0,0.5) = -0.5$$
$$f(0,3,0) = 2$$

Thus we can not only know if the particle is intersecting with the solid but also get the distance of the particle position to the nearest point on the solid, thus we can compute the minimum magnitude of the compensation displacement in the next time step.

6 ACKNOWLEDGEMENT

To Professor Dinesh K. Pai, for explaining basics of the formulations and the help for refining the final implementation.

7 REFERENCES

Baraff, D. and Witkin, A. 1998. Large steps in cloth simulation. In *Proceedings of SIGGRAPH 98*, ACM Press / ACM SIGGRAPH, Computer Graphics Proceedings. Annual Conference Series, ACM, 43-54.

Choi, K., AND Ko, H. 2002. Stable but responsive cloth. In *ACM Transactions on Graphics*, Volume 21, Issue 3.

Gere, J. M. 2001. *Mechanics of Materials*. Brooks/Cole.